Preprints of the 21st IFAC World Congress (Virtual)
Berlin, Germany, July 12-17, 2020

Improvements and Detailed Evaluation of Ground Obstacle Position, Size and Orientation Estimation ⋆

Peter Bauer *

* *Systems and Control Laboratory, Institute for Computer Science and Control (SZTAKI), Budapest, Hungary (e-mail: bauer.peter@sztaki.hu).*

Abstract: This paper improves and evaluates in detail a previous work of the author dealing with position, size and orientation estimation of fixed ground obstacles in aircraft sense and avoid. The improvement is the better conditioning of the system of equations by the shift of one known variable. Detailed evaluation means Monte-Carlo simulation and comparison of the disc and line-based parameter estimation methods considering also non-straight own aircraft trajectories. This is the focal point of the article as only straight trajectory results were compared until now. The mean estimation errors (in percentages) and their standard deviations with the two different methods are compared. Finally, the line-based method was better applicable for rectangular objects as expected.

Keywords: Obstacle detection, Ground obstacle, Position estimation, Size estimation

1. INTRODUCTION

In case of low level flight with small UAVs the avoidance of ground obstacles - such as transmission towers, tower-cranes, smokestacks or even tall tress - can be an important task of the on-board sense and avoid (S&A) system. An additional task can be the avoidance of ground vehicles and buildings during landing or in case of emergency landing.

This is underlined by literature sources such as Kikutis et al. (2017), Esrafilian and Taghirad (2016), Shahdib et al. (2013), Saunders et al. (2009) which propose different methods for ground obstacle position and size estimation and also avoidance.

The author of the current article has extended his work with aerial obstacles (Bauer et al. (2019)) to steady ground obstacles in Bauer et al. (2018) assuming constant own velocity, straight flight trajectories and disc-like obstacle cross sections. That work was extended for obstacles with rectangular cross section and time-varying own velocity and non-straight trajectories in Bauer (2019) but test results were provided only for constant velocity and straight trajectories because of space constraints of the paper.

The current work improves the previously proposed method with a modification to guarantee better conditioning of the resulting system of equations and presents detailed test results for non-straight trajectories and so time-varying velocity also. The number of examined obstacle types is also extended by two new.

⋆ This paper was supported by the János Bolyai Research Scholarship of the Hungarian Academy of Sciences. The research presented in this paper was funded by the Higher Education Institutional Excellence Program.

The structure of the paper is as follows. Section 2 shortly summarizes the proposed method from the previous work (Bauer (2019)). Section 3 discusses the conditioning problem and the proposed solution. Section 4 introduces the SIL simulation and evaluates the test results. Finally, Section 5 concludes the paper.

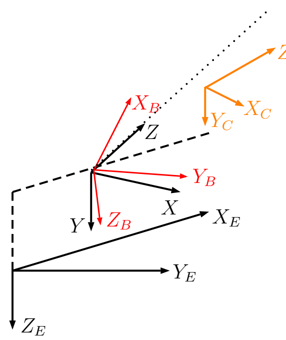

Fig. 1. The applied coordinate systems

2. SUMMARY OF PREVIOUS RESULTS

The applied coordinate systems are summarized in Fig. 1. X_E, Y_E, Z_E is the Earth (assumed to be fixed, non-moving, non-rotating), X, Y, Z is the trajectory (Z axis parallel with the straight trajectory (dotted line)), X_B, Y_B, Z_B is the body (moves and rotates together with the aircraft) and X_C, Y_C, Z_C is the camera coordinate system (with fixed position and orientation relative to the body system and forward pointing Z_C optical axis). Note that also in case of non-straight motion it is assumed that there is an intended flight direction which gives the trajectory system orientation.

Copyright lies with the authors

The disc projection model shown in Fig. 2 and applied in previous works of the author considers the tangents of the assumed horizontal disc cross section of the object in deriving the relations between object size and distance. However, this can lead to false size estimates if the projection of a rectangle is done as for example the projected size is a scaled combination of sides 1 and 2 in the figure.

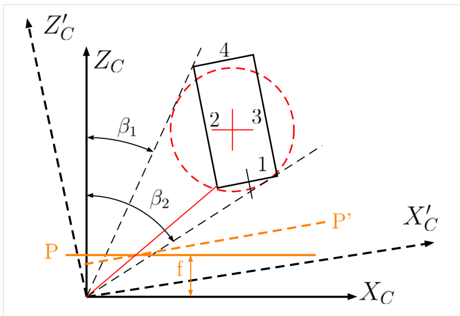

Fig. 2. Projection of disc or rectangle

To obtain better results for rectangular objects the projection of the linear edges should be considered. Assuming flat ground and that the object edges were detected its easy to determine object orientation relative to the trajectory system considering the vanishing point along the trajectory ($(0,0)$ image point in the camera system aligned with trajectory direction). The edge of the object is parallel with the aligned camera Z_C axis if it points into the $(0,0)$ point. A method to determine the required virtual camera rotation angle β_C is presented in Bauer (2019) in detail starting with the alignment of camera measurements with trajectory system.

After the virtual camera system alignment (shown with dashed coordinate system aligned with edge 1 in Fig. 2), relations between projected object size and distances should be derived. The derived relations also consider time-varying velocity and non-straight trajectories and are summarized in (1).

$$\underbrace{\begin{bmatrix} \frac{\{2\}f}{S_x(k)} \\ \frac{\{2\}x_k}{S_x(k)} \end{bmatrix}}_{LHS_k} = \begin{bmatrix} s\beta_C & c\beta_C & -\Delta X_k s\beta_C - \Delta Z_k c\beta_C \\ c\beta_C & -s\beta_C & -\Delta X_k c\beta_C + \Delta Z_k s\beta_C \end{bmatrix} \begin{bmatrix} \frac{X_0}{W} \\ \frac{Z_0}{W} \\ \frac{1}{W} \end{bmatrix} \qquad (1)$$

Here, S_x is the horizontal size of the disc or line image in the image plane (P), x is the horizontal position of the center of image or line, f is camera focal length, the multiplier $\{2\}$ is required if one considers disc model, X_0, Z_0 are the initial aircraft positions relative to the object in trajectory system, W is the real characteristic size of the object (disc model diameter or line length) and $\Delta X_k, \Delta Z_k$ are displacements of aircraft relative to the initial point after object detection. The actual aircraft position relative to the object in trajectory system can thus be characterized as $X_k = X_0 - \Delta X_k$, $Z_k = Z_0 - \Delta Z_k$. k identifies the considered t_k time instant. (1) gives two equations with three unknowns so at least two time samples are required to have a solvable system of equations.

Of course, in practical application its worth to consider multiple samples with a moving window technique.

If one considers the other side of the rectangle L (if its also detectable) its size can be determined as:

$$L_k = S_2(k)((X_0 - \Delta X_k)c\beta_C - (Z_0 - \Delta Z_k)s\beta_C \pm W/2)f \quad (2)$$

Here S_2 is the size parameter related to the second rectangle side in the image (for details see Bauer (2019)).

The absolute ground relative height H can be determined at t_k considering camera focal length and knowing the vertical coordinate of object top point y_T from the image (in the trajectory system), the actual flight altitude of aircraft h and the actual aircraft position as:

$$H_k = h_k - \frac{y_T(k) Z_k}{f} \qquad (3)$$

Taking a moving average for multiple time instants can decrease the variation of the estimated value.

3. IMPROVED CONDITIONING OF SYSTEM OF EQUATIONS

Considering the structure of the columns of the coefficient matrix in (1) and multiple sample times gives:

$$\begin{bmatrix} LHS_k \\ LHS_{k+1} \\ \vdots \\ LHS_{k+N} \end{bmatrix} = \underbrace{\begin{bmatrix} v_1 & v_2 & -v_1\Delta X_k - v_2 \Delta Z_k \\ v_1 & v_2 & -v_1\Delta X_{k+1} - v_2 \Delta Z_{k+1} \\ \vdots & & \\ v_1 & v_2 & -v_1\Delta X_{k+N} - v_2 \Delta Z_{k+N} \end{bmatrix}}_{M_k} \begin{bmatrix} \frac{X_0}{W} \\ \frac{Z_0}{W} \\ \frac{1}{W} \end{bmatrix} \qquad (4)$$

Where $v_1 = \begin{bmatrix} s\beta_C \\ c\beta_C \end{bmatrix}$, $v_2 = \begin{bmatrix} c\beta_C \\ -s\beta_C \end{bmatrix}$, N is the number of samples considered in the moving window. This shows that the third column is a linear combination of the first two but with time varying coefficients $\Delta X_k, \Delta Z_k$. This basically guarantees linear independence of the columns of the matrix but there are cases when the conditioning can get worse.

As ΔX_k is the cross distance from the trajectory system Z axis and ΔZ_k is the distance flown from Z_0 along this axis if ΔX_k is small or even zero and the aircraft approaches the obstacle the ΔZ_k values get close to Z_0 and so to each other:

$$\Delta Z_n \approx \Delta Z_{n+1} \approx \ldots \approx \Delta Z_{n+N} \approx Z_0 \qquad (5)$$

Here $n > k$ is assumed so these values are later in time than the values in (4). In this case the matrix can get close to singular as the coefficients of v_2 are almost the same and of v_1 are small or zero. This possible numerical problem can be avoided if one reformulates the system of equations.

Representing the initial aircraft position as $Z_0 = Z_0^k + \Delta Z_k$ leads to:

$$
\begin{aligned}
&Z_n = Z_0 - \Delta Z_n = Z_0^k + \Delta Z_k - \Delta Z_n = Z_0^k - \Delta Z_{n,k} \\
&0 < \Delta Z_{n,k} = \Delta Z_n - \Delta Z_k < \Delta Z_n
\end{aligned}
\tag{6}
$$

Considering $Z_0 = Z_0^{k-1} + \Delta Z_{k-1}$ and the definition of $\Delta Z_{n,k}$ leads to the following right hand side in (4):

$$
\begin{bmatrix}
v_1 & v_2 & -v_1 \Delta X_k - v_2 \Delta Z_{k,k-1} \\
v_1 & v_2 & -v_1 \Delta X_{k+1} - v_2 \Delta Z_{k+1,k-1} \\
\vdots & & \\
v_1 & v_2 & -v_1 \Delta X_{k+N} - v_2 \Delta Z_{k+N,k-1}
\end{bmatrix}
\begin{bmatrix}
\frac{X_0}{W} \\
\frac{Z_0^{k-1}}{W} \\
\frac{1}{W}
\end{bmatrix}
\tag{7}
$$

In this system the solution gives $\frac{Z_0^{k-1}}{W}$ and the value of Z displacements is limited to the displacement between t_k and t_{k+N} instead of t_1 and t_{k+N}. This way the ΔZ values can not be approximately equal and so the conditioning is better. Note that in case of fixed displacement Δz between every time step $\Delta Z_{k,k-1}$ to $\Delta Z_{k+N,k-1}$ transforms to:

$$
\Delta z \neq 2\Delta z \ldots \neq N\Delta z \neq Z_0 \tag{8}
$$

From Z_0^{k-1} its easy to calculate $Z_0 = Z_0^{k-1} + \Delta Z_{k-1}$.

Finally, a continuous shifting strategy can be constructed after the moving data window is first filled. In the future steps all of the stored data can be shifted by the ΔZ_{k-1} value which was just removed from the moving window leading to (7) in every step.

The effect on the condition number of the M_k matrix is shown in Fig. 3 from one of the Matlab simulations showing that without this shifting strategy the condition number can be as large as 275 while shifting limits it to about 22.

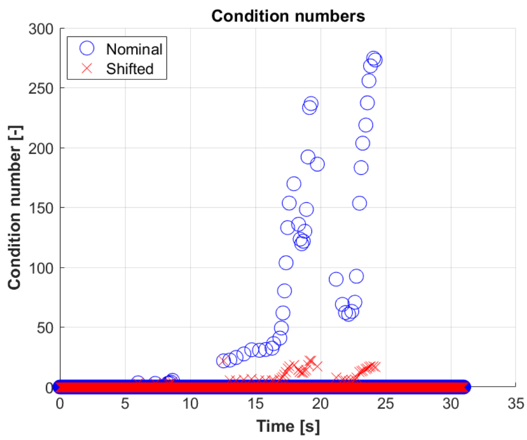

Fig. 3. Condition numbers without (Nominal) and with (Shifted) shift

4. SIL SIMULATION AND RESULTS

As in the previous works (Bauer et al. (2018), Bauer (2019)) an extensive SIL test campaign was run to evaluate the proposed method. A UAV following different trajectories with constant velocity (17m/s) was simulated in Matlab Simulink considering both aircraft and autopilot dynamics. A two camera system was modeled to extend overall horizontal field of view (FOV). Each camera has 70° horizontal and vertical FOV and $f = 914$ focal length and changes in the observing camera during maneuvering was handled. The considered objects are cylinder (tower), car (as in Bauer et al. (2018)), truck, long truck, house and large building. The detailed parameters can be seen in Table 1 together with short identifiers of objects (W, L are first and second side sizes and H is obstacle height). Object projection was done applying pinhole camera model with pixelization error based-on point cloud in case of cylinder or the corners in case of other objects. The simulation runtimes (and so initial distance Z_0) were different as shown also in the table. Image frequency was considered to be 8fps as this is the capability of state-of-the-art on-board hardware (see Bauer et al. (2019) about real flight S&A experiments). The flight altitude at the object was $1.5H$ except for the cylinder where it was H to test the effects of flying exactly at obstacle height for one object. The non-straight trajectories were generated with a doublet series course angle reference (with amplitudes $\Delta\chi = 0°, 10°, 20°$) causing left/right deviations from the straight trajectory as Fig. 4 shows. Note that straight trajectories are also considered in these test runs. Objects were placed with different side distances X_0 relative to their first side size ($X_0 = [0,\ 5,\ 10]\,W$) and different orientations ($\alpha = [0°,\ 15°,\ 30°,\ 45°]$) both relative to trajectory system. Of course the cylinder is tested only with one orientation. All tests were run with two glide slope values $0°/6°$ (horizontal flight and descend) giving 72 test runs for the rectangular objects and 18 for the cylinder.

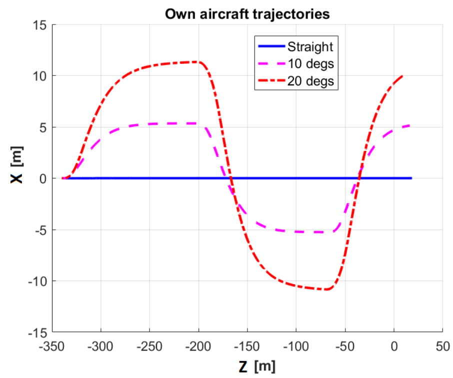

Fig. 4. Own aircraft trajectories

Table 1. Object parameters

ID	Object	W [m]	L [m]	H [m]	Run [s]
O1	Cylinder	6	6	30	20
O2	Car	1.7	4.5	1.45	20
O3	Truck	2.5	7	2.5	25
O4	Long truck	2.5	18	4	25
O5	House	15	15	8	30
O6	Building	15	40	89	50

The uncertainty in edge detection was modeled considering it only if the observed edge length was above 10 pixels. Possibility to calculate object orientation was considered if the difference of vertical edge end point coordinates was larger than 2 pixels. Line projection model was considered only if both edge detection and orientation calculation were possible. Disc projection model was used all the time to be able to compare the two methods. Solution of the system of equations (7) was done if the first 8 data points were collected. A moving window was applied after the first 8 data points.

After running the tests detailed evaluation was done. As there are strict conditions for line calculation (edge detection and possibility of angle calculation) its execution was not possible in every test case. Thus Table 2 summarizes how many successful line calculation cases occurred from the 72 test runs / object. The table shows that as the car is small there are several cases when line calculation was impossible (30 out of 72). With the other objects only a few cases are missing and for the house all cases succeeded. In case of the building the object is out of camera FOV before line calculation becomes possible in some cases.

Table 2. NR of cases when line calculation was possible

O1	O2	O3	O4	O5	O6
N/A	42	68	66	72	67

Another important information is the time during which the method is able to give information about the obstacle. The last 1 second before reaching the obstacle was neglected as any decision about the collision in this time is too late. So the tracking times were calculated from the time of first valid estimates (which means that the first 8 data points were collected) until 1 second before reaching the obstacle. The results for all object types (different line colors in figure) and line and disc method are shown in Fig. 5. The figure shows that while the disc method provides at least 5 seconds tracking time in every case the line method also has tracking times close to zero. This can probably get better in real cases depending on the capabilities of the edge detection algorithm (now the artificial 10 point length limit was introduced to decide about detected edge) and it is advisable to use disc calculation data until edges are detected.

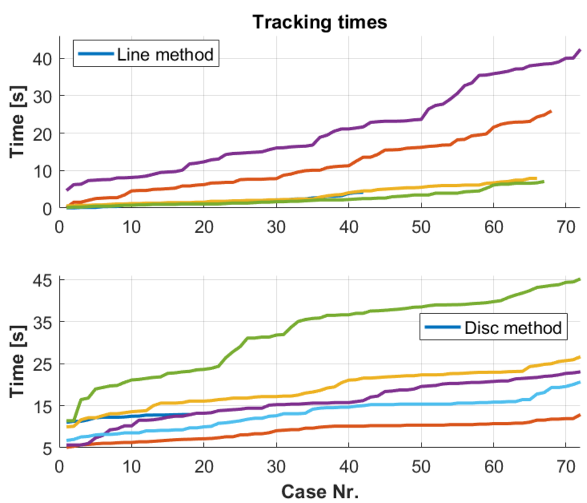

Fig. 5. Tracking times with line or disc method

The estimation errors of the parameters were determined in percentages at every time step relative to the real data. To make this enormous amount of data presentable the means and standard deviations of the absolute percentage errors were calculated for every run case.

Table 3. Cylinder error statistics (absolute %)

Cylinder	Z_0	X_0	W	L	α	H
Disc mean 90%	1.62	0.96	2.06	N/A	N/A	0.527
Disc STD 90%	2.47	12.87	9.83	N/A	N/A	2.58
Disc mean 50%	1.337	0.477	1.06	N/A	N/A	0.04
Disc STD 50%	1.89	0	5.54	N/A	N/A	0.28

Table 4. Car error statistics (absolute %)

Car	Z_0	X_0	W	L	α	H
Disc mean 90%	9.53	53.0	37.8	N/A	N/A	101.7
Disc STD 90%	10.76	40.06	49.45	N/A	N/A	71.18
Disc mean 50%	3.19	22.24	5.42	N/A	N/A	12.7
Disc STD 50%	4.61	0	23.0	N/A	N/A	13.13
Line mean 90%	0.76	9.47	6.36	8.4	0.95	54.6
Line STD 90%	0.91	5.85	5.81	6.05	0	25.24
Line mean 50%	0.25	3.4	2.62	2.63	0.32	10.37
Line STD 50%	0.08	0	1.23	0	0	0.23

Table 5. Truck error statistics (absolute %)

Truck	Z_0	X_0	W	L	α	H
Disc mean 90%	10.04	48.35	36.66	N/A	N/A	68.88
Disc STD 90%	13.57	40.3	55.22	N/A	N/A	59.86
Disc mean 50%	2.75	12.36	4.54	N/A	N/A	12.61
Disc STD 50%	4.9	0	17.32	N/A	N/A	18.74
Line mean 90%	0.52	11.13	3.7	4.67	0.72	19.46
Line STD 90%	1.74	20.9	7.86	8.6	1.13	26.35
Line mean 50%	0.19	1.2	1.6	1.77	0.22	5.89
Line STD 50%	0.36	2.19	3.73	4.13	0	2.34

Table 6. Long truck error statistics (absolute %)

Long truck	Z_0	X_0	W	L	α	H
Disc mean 90%	19.02	130	90.15	N/A	N/A	93.86
Disc STD 90%	38.36	147	106	N/A	N/A	136
Disc mean 50%	5.13	32.24	5.41	N/A	N/A	16.79
Disc STD 50%	12.41	0	39.5	N/A	N/A	26.44
Line mean 90%	0.78	5.45	4.75	6.52	0.43	30.5
Line STD 90%	2.39	12.61	9.48	11.52	0.36	28.82
Line mean 50%	0.25	1.56	1.97	2.27	0.13	10
Line STD 50%	0.58	3.18	4.46	5.67	0	3.3

Table 7. House error statistics (absolute %)

House	Z_0	X_0	W	L	α	H
Disc mean 90%	8.58	20.02	22.32	N/A	N/A	43.72
Disc STD 90%	12.23	17.5	24.77	N/A	N/A	44.29
Disc mean 50%	2.15	12	3.76	N/A	N/A	6.72
Disc STD 50%	4.49	0	13.09	N/A	N/A	8.74
Line mean 90%	2.56	12.92	4.24	6.91	1.66	20.76
Line STD 90%	7.79	7.5	11.69	12.06	0	27.78
Line mean 50%	0.71	9.91	1.14	0.97	0.67	4.08
Line STD 50%	1.86	0	5.98	5.47	0	4.2

Table 8. Building error statistics (absolute %)

Building	Z_0	X_0	W	L	α	H
Disc mean 90%	13.6	124	43.1	N/A	N/A	29.6
Disc STD 90%	13.3	103	44.6	N/A	N/A	32.3
Disc mean 50%	4.23	24.98	5.23	N/A	N/A	9.12
Disc STD 50%	8.01	0	22.67	N/A	N/A	14.32
Line mean 90%	3.09	12.44	8.94	5.05	3.26	6.32
Line STD 90%	12.52	32.22	38.57	17.93	1.24	18.88
Line mean 50%	0.45	1.66	1.63	1	0.45	3.98
Line STD 50%	4.49	10.22	11.4	8	0	4.44

The mean errors of the different parameters are plotted in ascending order for all objects (different colors) and disc and line methods in Appendix A having the run number on the horizontal axis. The upper mean value and standard deviation (STD) limits for 90% and 50% of the valid cases of every object are summarized in Tables 3 to 8. These mean that 90% or 50% of the means or STDs is smaller than the given value.

Analysing the tables shows that the disc method gives 1-2% mean estimation error with 3-13% STD for the cylinder object in 90% of the cases as it fits the model in the method. For rectangular objects this performance decreases to 10-130% mean error with 10-150% STD which clearly shows that the applicability of the disc method for rectangular objects is very limited. Of course, considering only 50% of the cases highly decreases these values as the tables show. For the Z_0 initial distance the disc method gives 10% mean with 10% STD for 90% of the data which is acceptable but for the other parameters (X_0, W, H) 20% and even higher than 100% mean errors can be found which can be unacceptable.

Considering the line method the mean errors are below 13% for 90% of the data except for the obstacle height (H) parameter where 7-55% mean values result for 90% of the data except for the cylinder case. The cause of this uncertainty is the flight altitude which is always above the top of the obstacle except for the cylinder. In $1.5H$ cases the top coordinate of the obstacle is the mean of the corner values and this an inaccurate measurement. This should be improved later. The STD values for the line method are 6-33% for 90% of the data which can be acceptable. Considering the separate parameters the line method always gives better means and STDs than the disc method. Its worth to note that the mean errors for the W and L sides are the same and the mean errors (0.5-4%) and STDs (0-2%) of the object orientation (α) estimation are very low which shows that the orientation estimation works pretty well.

Finally, its worth to note that initial transients can occur in the parameter estimates and they were not excluded from the calculations so STDs for both disc and line methods can be much lower considering only the converged results.

5. CONCLUSION

This paper continues the work of a previous paper of the author where ground obstacle position, size and orientation estimation methods were presented for cylindrical (disc projection model) and rectangular (line projection model) obstacles and compared for straight flight trajectories of the own aircraft. The current work introduces an improvement which can limit the condition number of the resulting system of equations, extends the considered test objects with car and house and runs Monte-Carlo test simulation with non-straight own flight trajectories to evaluate the methods also for these cases. The absolute mean percentage errors of the parameter estimates and their standard deviations are calculated and compared for the disc- and line-based methods. As an overall summary it can be stated that the line method outperforms the disc method in case of rectangular objects (see the tables and also the mean error plots in Appendix A) as expected so its worth to build a ground obstacle sense and avoid strategy considering also this method. A limitation of the line-based method is the requirement to detect object edges which can delay parameter calculation as the aircraft approaches the object. This can significantly decrease the tracking time of the object and so the time for decision about collision however, the disc-based method can be used before. For distant objects the difference between disc-based and line-based results can be negligible so this is a feasible approach. Another limitation of both methods is the need for a given trajectory direction around which the aircraft trajectory changes. Further improvements are required to handle completely free trajectories. As obstacle height estimation has the least precision its further improvement is also required.

REFERENCES

Bauer, P. (2019). Position, Size and Orientation Estimation of Ground Obstacles in Sense and Avoid. In *In Proc. of 21st IFAC Symposium on Automatic Control in Aerospace, ACA 2019.*

Bauer, P., Hiba, A., and Zsedrovits, T. (2019). Real Flight Application of a Monocular Image-Based Aircraft Collision Decision Method. *International Journal of Aerospace Engineering*, 2019, 16. doi:10.1155/2019/7191839. URL `https://doi.org/10.1155/2019/7191839`.

Bauer, P., Vanek, B., and Bokor, J. (2018). Monocular Vision-based Aircraft Ground Obstacle Classification. In *In Proc. of European Control Conference 2018 (ECC 2018)*, 1827–1832.

Esrafilian, O. and Taghirad, H.D. (2016). Autonomous flight and obstacle avoidance of a quadrotor by monocular slam. In *2016 4th International Conference on Robotics and Mechatronics (ICROM)*, 240–245. doi:10.1109/ICRoM.2016.7886853.

Kikutis, R., Stankunas, J., Rudinskas, D., and Masiulionis, T. (2017). Adaptation of Dubins Paths for UAV Ground Obstacle Avoidance When Using a Low Cost On-Board GNSS Sensor. *Sensors*, 17(10), 1–23.

Saunders, J., Beard, R., and Byrne, J. (2009). Vision-based reactive multiple obstacle avoidance for micro air vehicles. In *2009 American Control Conference*, 5253–5258. doi:10.1109/ACC.2009.5160535.

Shahdib, F., Wali Ullah Bhuiyan, M., Kamrul Hasan, M., and Mahmud, H. (2013). Obstacle detection and object size measurement for autonomous mobile robot using sensor. *International Journal of Computer Applications*, 66, 28–33. doi:10.5120/11114-6074.

Appendix A. MEAN ESTIMATION ERRORS

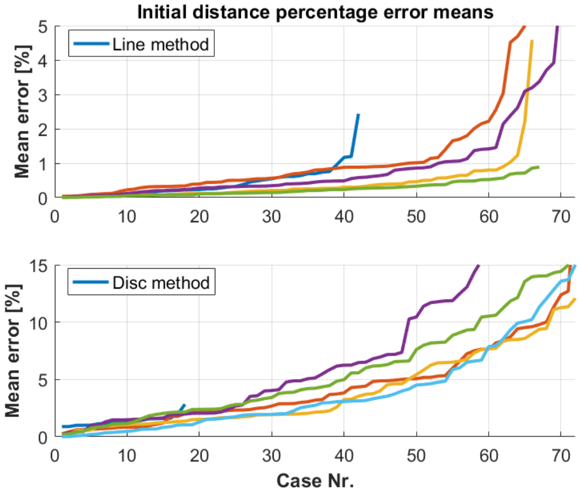

Fig. A.1. Mean errors of initial distance (Z_0) estimate

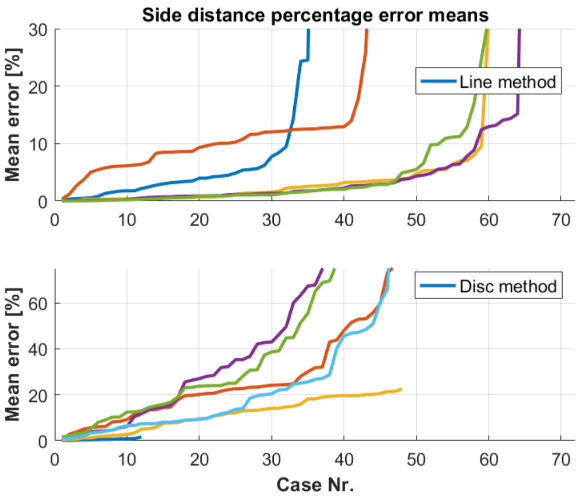

Fig. A.2. Mean errors of initial side distance (X_0) estimate

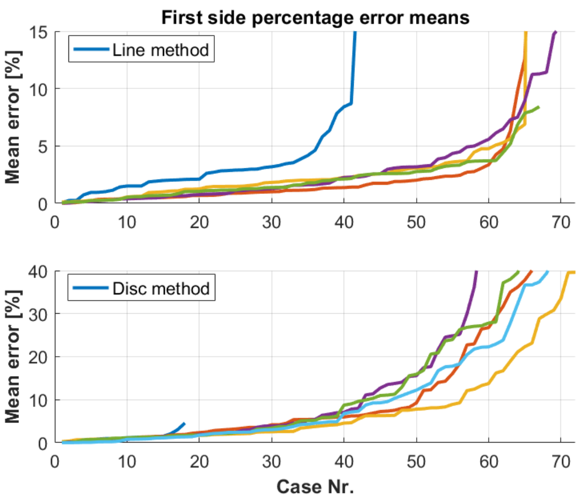

Fig. A.3. Mean errors of first side (W) estimate

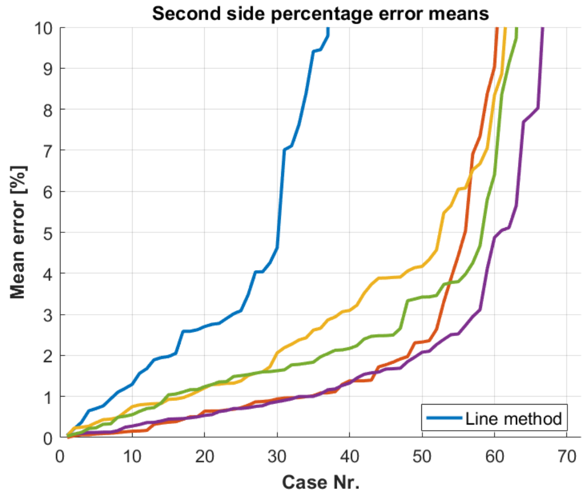

Fig. A.4. Mean errors of second side (L) estimate

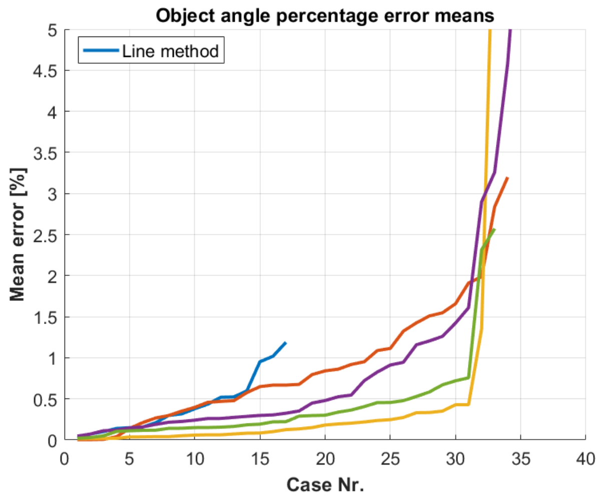

Fig. A.5. Mean errors of obstacle angle (α) estimate

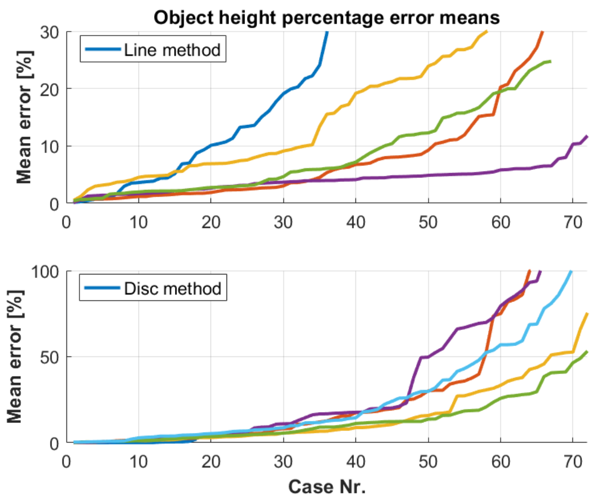

Fig. A.6. Mean errors of obstacle height (H) estimate